Observation of collective excitations in MgZnO/ZnO two-dimensional electron systems by resonant Raman scattering

A. B. Van'kov, B. D. Kaysin, V. E. Kirpichev, V. V. Solovyev, and I. V. Kukushkin
Institute of Solid State Physics, Russian Academy of Sciences, Chernogolovka 142432, Russia
(Received 21 June 2016; revised manuscript received 4 September 2016; published 19 October 2016)

The neutral excitations in two-dimensional electron systems (2DES) confined at $Mg_xZn_{1-x}O/ZnO$ heterojunctions were studied by a resonant inelastic light scattering (ILS) technique. At zero magnetic field the ILS spectra of intra- and intersubband collective excitations are detected in the wavelength range close to the ZnO direct band gap. The intersubband spectrum is represented by collective modes of charge- and spin-density excitations along with single-particle excitation continuum. The energies of these excitations were characterized on the series of samples and shown to grow sublinearly with the two-dimensional electron density. The intrasubband 2D plasmon was observed at plasma frequency and its square-root momentum dispersion was ascertained. Strong electron-electron correlations are manifested in the energy structure of intersubband excitations. Depolarization and excitonic contributions to the charge- and spin-density excitation energies are extracted in the wide range of 2D-electron densities. The negative excitonic contribution dominates among the many-particle energy terms and results in an unusual hierarchy of 2DES intersubband collective excitation energies.

DOI: 10.1103/PhysRevB.94.155204

I. INTRODUCTION

Recent breakthroughs in the growth technology of ZnO-based semiconductor heterostructures [1,2] open novel opportunities for fundamental studies of strongly correlated two-dimensional electron systems (2DES). Thanks to its material parameters, ZnO-based electron systems are characterized by unprecedentedly large interaction parameter with values of $r_s \approx 15$ readily accessible, this also goes in combination with comparable magnitudes of the cyclotron energy and the Zeeman energy. Ultrahigh electron mobilities of the order 10^6 cm^2/V s in ZnO structures [3] have enabled manifestation of the rich variety of the collective phenomena. Examples are the strong renormalization of the spin susceptibility and effective mass, exotic fractional quantum Hall states [4]. Reduction of electron density enables rearrangement of spin-split Landau levels and realization of Stoner ferromagnetism [5].

Energy scales governing the electronic spectrum, as well as many-particle correlations, are all manifested in the structure of collective excitations. One of the most effective tools for exploring neutral electronic excitations is an inelastic light-scattering (ILS or Raman scattering) technique which allows one to reconstruct the full spectrum of low-energy excitations. As it has been shown in numerous optical studies of GaAs-based two-dimensional electron systems, the ILS spectra may be detected under resonant photoexcitation in the vicinity of the direct band gap. They reveal a multitude of intra- and intersubband excitations depending on the ground state of the system, the applied perpendicular magnetic field, spin ordering, and other parameters [6–8]. Probing electronic excitations in ZnO-based two-dimensional (2D) electron systems by ILS is thus a promising way of studying their energy spectrum and nontrivial collective effects therein.

Until now, most of the reported optical investigations of ZnO-based materials have been conducted using photoexcitation from discrete UV lines of gas lasers [9–11]. However, at an arbitrary laser excitation, the scattering efficiency of the ILS process is vanishingly small and therefore discrete wavelength lasers are generally not suitable for exploring Raman scattering from low-dimensional electronic systems. In that case a resonantly enhanced inelastic light scattering may help. This resonant technique has been previously applied to ZnO structures for detection of bulk LO phonons in the vicinity of excitonic resonances [12].

Here, a resonant Raman technique is utilized to study collective excitations of 2D electrons in ZnO. A number of spectral lines, corresponding to intersubband and intrasubband excitations, are found and identified at zero magnetic field. The only visible intrasubband collective excitation is a 2D plasmon, detected at plasma energy. The intersubband excitations are represented by two collective excitations of charge and spin density and a single-particle continuum. Energies of all intersubband excitations were systematically measured as a function of electron density and associated changes in the confinement potential. Surprisingly, the single-particle excitation continuum is found at energies exceeding those of both collective modes. The many-particle energy terms, such as depolarization shift and excitonic shift, are extracted from experimental data on intersubband excitations.

II. EXPERIMENTAL TECHNIQUE

The studies were conducted on a set of nine $Mg_xZn_{1-x}O/ZnO$ heterostructures, grown by liquid-ozone assisted molecular beam epitaxy [2]. Structures have been characterized using low-temperature ($T = 0.3$ K) magneto-transport measurements to extract electron mobilities and densities. Although different pieces (without Ohmic contacts) of those wafers were used for optical experiments, their electron densities were determined *in situ* by means of a magneto-photoluminescence (magneto-PL) technique (see below). The actual sample parameters are listed in Table I. Most of the inelastic light-scattering measurements were performed on sample 426 with rather high mobility and good visibility of the Raman signal. Other samples were used primarily with the aim of variation of an electron density parameter.

TABLE I. The parameters of the 2DES in the set of studied samples, ordered by increasing of electron density. The electron density n_s was measured using the magneto-photoluminescence technique. Mobility μ_t was qualified by magnetotransport measurements.

Sample ID	n_s (10^{11} cm^{-2})	μ_t (10^3 cm^2/V s)
254	1.1	?
259	1.8	?
244	2.3	400
427	2.8	427
426	3.5	410
448	4.5	250
466	4.8	250
302	6.5	200
479	11.2	80

The resonant photoexcitation was produced by a tunable laser source operating in the vicinity of direct interband optical transitions of ZnO. It was designed as a frequency-doubled tunable continuous-wave Ti-sapphire laser with output monochromatic radiation in the wavelength range 365–368 nm. Barium borate crystal was utilized as a nonlinear element, working in the single-pass configuration. The typical UV excitation power was 2–7 μW, which was delivered to the sample by a 400-μm glass fiber and distributed over a spot of $\sim$1 mm^2. Thus the excitation power density was well below 1 mW/cm^2 and excluded heating of the 2D electrons. Optical spectra were detected using a spectrometer conjugated with a liquid-nitrogen-cooled CCD camera. In the UV range the system had a linear dispersion of 5 Å/mm and a spectral resolution of 0.3 Å.

Measurements were conducted at low temperatures in the range 0.3–0.5 K in a cryostat with a superconducting solenoid. Inelastic light-scattering data were taken at zero magnetic field. Optical access to the sample was organized via two quartz fibers, one of which was used for photoexcitation and the other for signal collection. The in-plane momentum $k_{||}$, transferred to the 2DES, was determined by the angular configuration of the two fibers [shown in the inset to Fig. 3(a)]. At our experimental conditions $k_{||}$ ranged from 0.7×10^5 to 2×10^5 cm^{-1}. At one experimental stage the Raman spectral lines were tested by polarization selection rules. For this purpose two identical linear polarizers were placed between fiber tips and a sample surface in either parallel or orthogonal configurations to each other.

The magneto-PL technique has been utilized for navigation across the multitude of bulk and two-dimensional spectral features, present in PL spectra of MgZnO/ZnO heterostructures. A central idea here is that bulk and two-dimensional lines behave in a different manner while sweeping a normal component of an external magnetic field. Two-dimensional lines exhibit characteristic $1/B-$ periodic oscillations in intensity and/or in spectral position due to discretization of Landau levels. This feature was routinely used here (and in previous studies [10,13]) for *in situ* determination of the 2D-electron density in all studied samples. Furthermore, this characteristic behavior allowed one to specify several transitions involving 2D electrons in the two lowest subbands and states in A and B branches of valence bands [10].

Screening of the PL signal from 2D electrons is an immediate prerequisite to the search of any resonant inelastic light-scattering lines. As it has been demonstrated in previous works on GaAs heterostructures [14,15], the scattering efficiency from 2DES becomes enhanced by several orders of magnitude if the conditions of incoming and/or outgoing optical resonances are fulfilled. In practice, this works when the frequency of incident or scattered photon approaches any suitable 2D electron-hole transition energy. The resonant behavior of 2D-Raman lines serves as an additional selection rule, enabling one to discriminate bulk lines from ILS lines of 2D origin.

III. INTER- AND INTRASUBBAND EXCITATIONS IN RAMAN SPECTRA

Figure 1 shows a waterfall with optical spectra obtained on sample 426 with a 2DES density $n_s = 3.5 \times 10^{11}$ cm^{-2}, with changing the wavelength of the laser excitation. The gradual shift of the laser line is accompanied by an identical shift of the resonant Raman line marked by a dashed line, whereas the spectral position of the much more intense PL lines are left unchanged. At wavelengths around 3665–3667 Å one may see a notable increase of the Raman line intensity due to a resonant intersection with some optical transition in this range. The Raman line fades as the laser wavelength moves further outside of this band.

The most prominent Raman feature observed in Fig. 1 is denoted as CDE (for the reasons discussed below). Its Raman shift equals $\sim$13 meV and its linewidth is comparable to the spectrometer resolution limit of $\sim$0.3–0.4 meV. Similar behavior is also displayed by the Raman feature denoted by SPE, referring to spin-density excitation [see inset to Fig. 1(a)]. It is blueshifted by 2.6 meV with respect to the CDE line. Its intensity is enhanced while crossing the same optical transitions, but the best visibility obtainable is still much worse than that of the CDE line due to its broader spectral width (roughly $\sim$2 meV) and suppressed peak intensity. This behavior is illustrated in panel (b) of Fig. 1, where intensities of both lines are plotted as a function of laser wavelength. For the SPE Raman band the contour of resonant enhancement is blueshifted because of the difference in Raman shifts. An exemplary spectrum where CDE and SPE are detected simultaneously is shown in the inset of Fig. 1(a). Here, the CDE line is already well outside of the resonance and is only faintly visible.

Resonance conditions are naturally different for excitations of various origin. Hence, the systematic tuning of the laser excitation wavelength over a broad range in the neighborhood of PL lines offers a convenient procedure to search for all existing 2D-Raman lines. In this way two more Raman features, not present in the data displayed in Fig. 1, were found at longer laser excitation wavelengths [Figs. 2(b) and 3(b)]. Note that these spectra are given in a more appropriate Raman shift scale, where energies of collective excitations, rather than wavelengths of PL background, are emphasized.

The identification of the observed Raman lines of neutral electronic excitations can be easily performed at zero magnetic field. Previous studies [8,15,16] indicate that the Raman spectrum should contain branches of intrasubband and

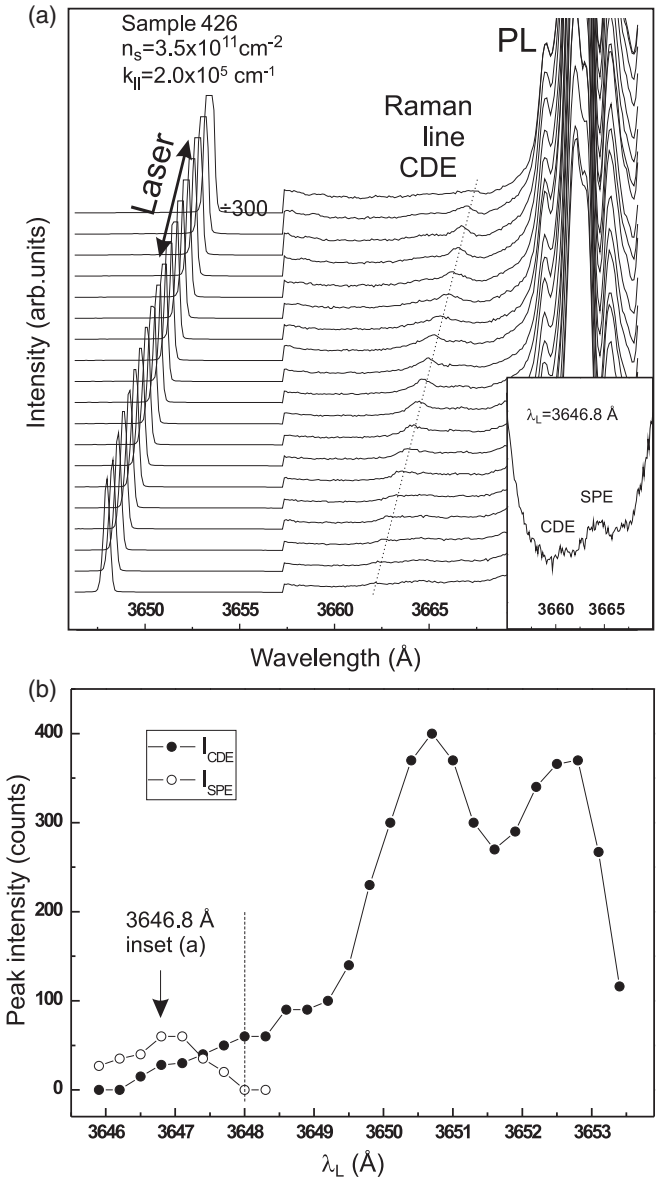

FIG. 1. (a) The evolution of the ILS optical spectrum as the laser wavelength is tuned. The Raman line, marked by a dashed line, tracks the laser line in a parallel manner. Its intensity is enhanced in the region between 3664 and 3667 Å. PL features on the right side preserve their spectral positions irrespective of the photoexcitation conditions. The *inset* shows a magnified view of the spectrum for $\lambda_L = 3646.8$ Å (outside the range of the main tableau). Both the SPE and the CDE Raman bands are present thereupon. (b) The profiles of resonant excitation for two Raman features CDE and SPE. Peak intensities of lines are plotted as a function of excitation laser wavelength. Data points to the left of a dashed vertical line are not shown on the waterfall of plot (a) due to a weak signal level. The arrow marks the position $\lambda_L = 3646.8$ Å, corresponding to the inset of panel (a).

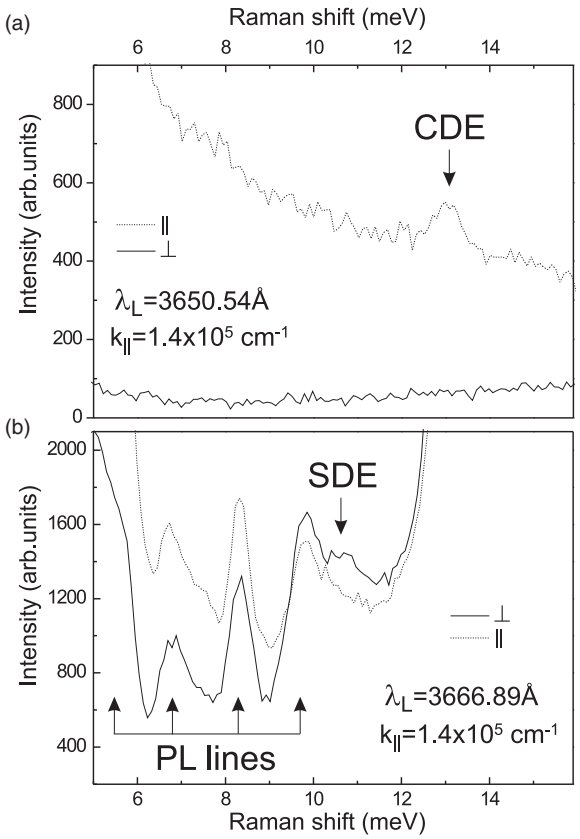

FIG. 2. Linearly polarized ILS spectra of intersubband collective excitations measured on sample 426 with $n_s = 3.5 \times 10^{11}$ cm^{-2}. Two Raman features, CDE and SDE, have been tested at different configurations of linear polarizers. In plot legends (||) means that incident and detected light beams are collinearly polarized, and for (⊥) spectra they are cross-polarized. The Raman feature CDE in panel (a) with a Raman shift of approximately 13 meV emerges exclusively in a collinear configuration of polarizers. According to the polarization selection rules, this is a true indication of the charge-density excitation. In contrast, the weak Raman feature at ∼10.9 meV, seen in the PL background in panel (b), is observed in cross-polarized configuration only and is therefore identified as a signal from spin-density excitation. Note, that owing to different resonant conditions, spectra are taken at different absolute laser positions, indicated on the corresponding panels.

intersubband excitations. The intersubband spectrum should consist of two collective modes—the charge- and spin-density excitations referred to as CDE and SDE, respectively, and a continuum of single-particle excitations (SPEs). A polarization selection rule can be applied to discriminate between the CDE and SDE [15]. The only intrasubband collective excitation involves 2D plasmon. It can be experimentally recognized both by the polarization selection rules and by its well-established square-root momentum dispersion.

Identification of two Raman features, CDE and SDE, has been performed by means of polarization selection rules. For that purpose two linear polarizers were applied to the incident and scattered light beams so that their polarizations were either parallel or orthogonal to each other. The panels in Fig. 2 show the influence of the polarization orientation on the visibility of CDE and SDE peaks measured on sample 426. On panel (a) one may see that Raman line CDE is detected only if incident and scattered photons have collinear polarizations. This justifies attribution of this line to the intersubband charge-density excitation. In contrast, the Raman line, marked

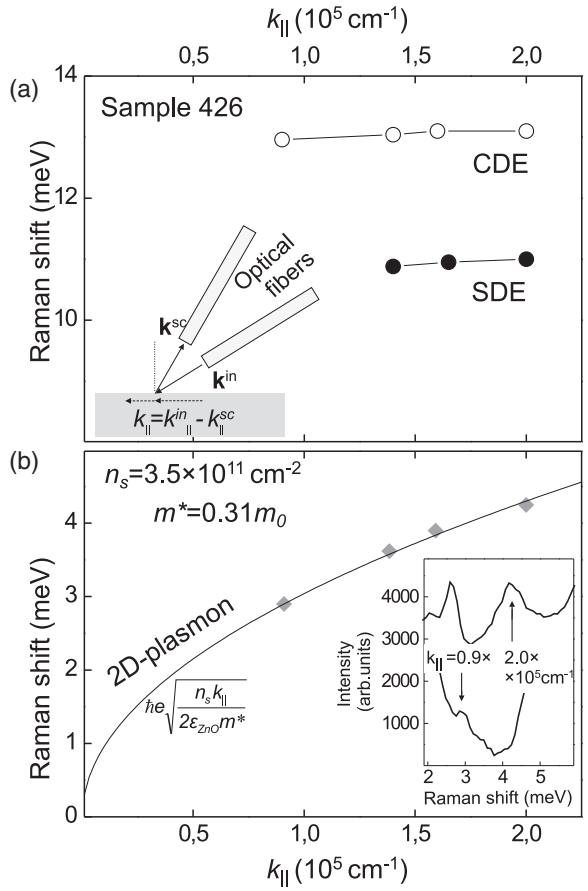

FIG. 3. (a) The dispersion of the CDE and SDE measured for small values of in-plane momentum by varying the angle of the optical fibers with respect to the sample surface. The sketch in the inset illustrates momentum transfer to the 2DES in the light-scattering process. (b) The dispersion of the intrasubband 2D-plasmon excitation. The curve represents calculated values of the plasmon dispersion assuming $m^* = 0.31\,m_0$ and $\varepsilon_{ZnO} = 8.5$). The inset shows two Raman spectra of 2D plasmon recorded at different transferred momenta $k_{||} = 0.9 \times 10^5$ cm^{-1} and $k_{||} = 2.0 \times 10^5$ cm^{-1}. The excitation laser wavelengths are $\lambda_L = 3665.9$ Å and $\lambda_L = 3663.63$ Å, respectively.

SDE, is observed in a cross-polarized configuration only. This confirms identification of this line as the spin-density excitation (SDE). Data for panels (a) and (b) were recorded at different laser wavelengths, since resonant conditions for these two collective excitations differ. Strong peaks surrounding the SDE line on panel (b) are all of photoluminescence origin, since their spectral positions are independent of laser position.

The collective excitations present in Raman spectra have also been tested with regard to their momentum dispersion. The process of momentum transfer to 2DES is illustrated in the inset of Fig. 3(a). Practically, the transferred momentum was adjusted by small discrete changes in orientations of optical fibers. In Fig. 3 we plot energies of identified Raman lines as a function of transferred in-plane momentum, measured on sample 426. Intersubband excitations CDE and SDE show no dispersion beyond the resolution limit of ~0.3 meV for the accessible $k_{||}$ values [Fig. 3(a)]. In contrast, the intrasubband excitation displays a notable momentum dispersion. The inset to Fig. 3(b) shows the two representative Raman spectra of intrasubband excitation, taken at different transferred momenta— $k_{||} = 0.9 \times 10^5$ cm^{-1} and $k_{||} = 2.0 \times 10^5$ cm^{-1}. The Raman shift of the excitation evidently grows with $k_{||}$. The four measured data points [Fig. 3(b)] perfectly fit the square-root dependence of energy on the momentum, a hallmark of the intrasubband 2D plasmon. There are two material parameters which influence the plasmon dispersion—the dielectric constant and the effective mass. For excitations with energies much smaller than LO and TO phonon energies the value of low-frequency or static dielectric constant is to be considered. This is known to be $\varepsilon_{ZnO} = 8.5$ (see, e.g., [5]). The effective mass in the conduction band has been accurately measured in the previous experiments based on the optical detection of the resonant microwave absorption by magnetoplasma excitations [11]. Those measurements gave effective cyclotron mass $m^* = 0.31\,m_0$ for a sample with electron density $n = 3.5 \times 10^{11}$ cm^{-2}, as in Fig. 3. The two parameters define the theoretical dispersion law of 2D plasmon, plotted with a solid curve in Fig. 3(b). The coincidence of experimental and theoretical data points in Fig. 3(b) reliably confirms the identification of the plasmon spectral line.

The energies of intersubband excitations substantially exceed those of intrasubband plasmon. Charge- and spin-density excitations have been detected from nearly all samples from Table I, except one structure, where the SDE line has not been resolved due to poor electron mobility and/or strong PL background. As it is known from studies of intersubband excitations in high-quality GaAs/AlGaAs heterostructures [15,16], apart from collective intersubband excitations a Raman spectrum contains a contribution from a single-particle excitation continuum, spread around the bare intersubband splitting energy E_{10}. Its spectral width extends within the energy interval from $E_{10} - v_F \hbar k_{||}$ to $E_{10} + v_F \hbar k_{||}$. Inserting the relevant experimental parameters such as the electron density ~5×10^{11} cm^{-2} and the transferred in-plane momentum ~1.5×10^5 cm^{-1}, the SPE Raman signal is expected to have a width of about 1.5–2 meV, close to our experimental findings. The SPE Raman band was detected on just four structures, covering a density range from 3.5×10^{11} to 6.5×10^{11} cm^{-2}. In all cases it is visible at resonant conditions analogous to the CDE line and possesses energy higher than both intersubband collective modes.

IV. DISCUSSION

The data points on Fig. 4 summarize the dependence of excitation energies on the electron density over a span of an order of magnitude. Both CDE and SDE energies grow sublinearly with electron density. The trends can be fitted by power laws $E_{CDE} \approx n^{0.57}$ and $E_{SDE} \approx n^{0.55}$, with curves shown in Fig. 4(a). Qualitatively, these power laws are not far from the model dependence of intersubband splitting in inversion layers or triangular potential wells, $n^{2/3}$ (see, e.g., [17]). However, none of these approximations can be directly applied to $Mg_xZn_{1-x}O/ZnO$ heterostructures considering the complicated confinement potential [schematically illustrated in the inset to Fig. 4(a)]. The electron density in these

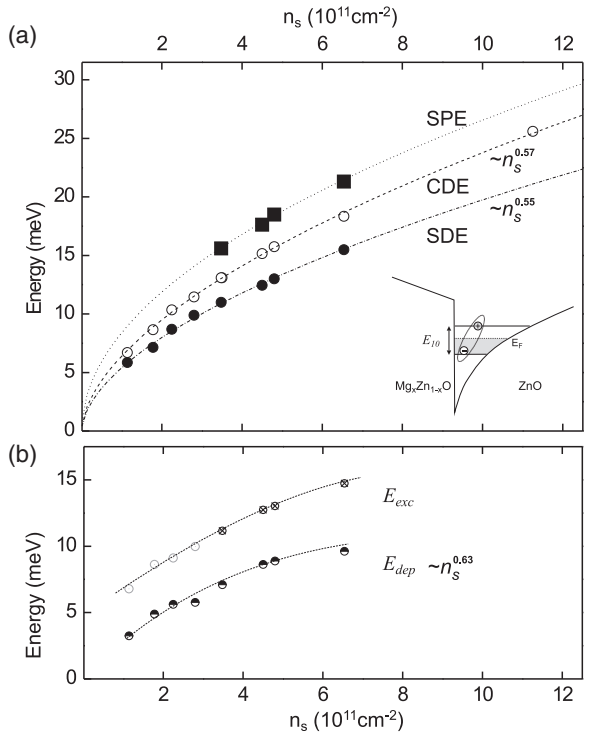

FIG. 4. (a) The energies of all three intersubband excitations measured on a set of MgZnO/ZnO heterostructures with varying electron density covering the range 10^{11}–10^{12} cm^{-2}. Open and solid circles represent the energy of the CDE and SDE. Squares indicate the energy of the SPE mode. The inset illustrates the confinement potential and subband energy levels in MgZnO/ZnO heterostructures. (b) Magnitude of the exciton binding and depolarization energy contributions to the energy of the SDE and CDE intersubband excitation modes. The values are extracted from the data contained in Fig. 4(b).

heterostructures is governed by a modification of the magnesium content in the barrier, x. Simultaneously, this entails tuning of the electric fields on both sides of the interface, the conduction-band discontinuity—all these parameters influence the subband energy levels in a complicated manner. Furthermore, many-particle terms contribute to the excitation energies significantly and may alter their dependence. Both CDE and SDE possess a negative excitonic shift, which is a binding energy of an electron in the first excited subband and a vacancy left in the lowest subband. This energy contribution is determined by the profiles of wave functions in subbands and scales with electronic Rydberg. For the CDE mode (or intersubband plasmon) a positive energy contribution, referred to as a depolarization shift, has to be taken into account. This yields [18]

$$E_{\mathrm{SDE}}^2 = E_{10}^2 - E_{\mathrm{exc}}^2, \quad E_{\mathrm{CDE}}^2 = E_{10}^2 - E_{\mathrm{exc}}^2 + E_{\mathrm{dep}}^2. \qquad (1)$$

Here E_{exc} and E_{dep} are the excitonic and depolarization shifts, respectively, and E_{10} is the bare intersubband splitting.

The experimental values of the excitonic (E_{exc}) and depolarization (E_{dep}) energies can be obtained from the data points in Fig. 4(b) using Eq. (1). The depolarization shift simply follows from $E_{\mathrm{dep}}^2 = E_{\mathrm{CDE}}^2 - E_{\mathrm{SDE}}^2$. It can be extracted for nearly the whole range of electron densities. Its density dependence is plotted in Fig. 4(a). It evidently tends toward zero as the density is lowered. The experimental trend can be fitted by the power law $\sim n_s^{0.63}$ (dashed line). The power index seems reasonable, since the depolarization shift is essentially the energy of plasma oscillations with an effective electron density $\sim n_s/\langle z\rangle$, where $\langle z\rangle$ is the characteristic width of subband wave functions. The dependence deviates from a square-root growth, because the width of the wave function shrinks with increasing density [10].

E_{exc} can be directly obtained from E_{SDE} and E_{SPE} for those four samples for which it was possible to detect the SPE signal. An extrapolation of E_{SPE} to lower densities has been used to estimate the excitonic shift at the other densities. This is justified, since E_{SPE} should exhibit a similar trend like the SDE and CDE energies.

From Fig. 4(a) we conclude that the excitonic shift significantly exceeds the depolarization shift across the whole range of electron densities. This leads to an unusual ordering of the intersubband excitations. Studies of the intersubband excitation spectrum on GaAs-based two-dimensional electron systems [15,16,18] have consistently revealed that the positive depolarization energy contribution exceeds the absolute value of the negative excitonic energy shift. Hence, in these systems the CDE and SDE modes flank above and below the SPE mode. In stark contrast, both the CDE and the SDE modes are located well below the SPE mode in ZnO-based heterostructures, which indicates the dominant contribution of the negative excitonic shift among the many-particle energy terms.

It is worth noting that the alternative approach utilizing photoluminescence and reflection techniques in [10] for probing the subband energy-level splitting in MgZnO/ZnO gave somewhat different results. Intersubband splittings extracted from *interband* electron-hole transition energies include corrections from excitonic binding energies. These depend on the overlap of the electron and hole wave functions and scale with the electron-hole Rydberg, rather than conduction-band electron-electron Rydberg. Hence, energies for conduction-band collective modes and for *interband* optical transitions have excitonic contributions of a different nature.

A quantitative theoretical description will require a theoretical approach dealing with collective excitations in a strongly interacting system. For the quasi-2D-electron systems being considered, Coulomb interaction is one of the leading energy scales, and consequently, no small interaction parameter could be introduced into a theoretical model. The local-density approximation and generalized random-phase approximation, successfully utilized for calculation of intersubband excitations in GaAs-based structures, are not directly applicable for electrons in ZnO.

To conclude, we have utilized the method of resonant inelastic light scattering to probe neutral electronic excitations in strongly interacting 2DES in MgZnO/ZnO heterostructures. At zero magnetic field both intra- and intersubband excitations have been detected and identified. Their dispersions have been explored by varying the transferred in-plane momentum. Intrasubband 2D plasma excitation has been recognized by its square-root momentum dispersion. Charge- and spin-density intersubband excitations were distinguished based on polarization selection rules. Their energies depend on

electron density in a sublinear manner, due to deformation of a confinement potential. Both of them show a negligible dispersion in the long-wave limit. The Raman band associated with the intersubband single-particle continuum was found at energies exceeding those of both collective intersubband modes. This is fundamentally different from the mode ordering in more familiar systems such as GaAs 2DES and is caused by large values of negative excitonic shift in ZnO dominating over other many-particle energy terms.

ACKNOWLEDGMENTS

We acknowledge financial support from the Russian Science Foundation (Grant No. 14-12-00693).

[1] Y. Kozuka, A. Tsukazaki, and M. Kawasaki, Appl. Phys. Rev. **1**, 011303 (2014).
[2] J. Falson, D. Maryenko, Y. Kozuka, A. Tsukazaki, and M. Kawasaki, Appl. Phys. Express **4**, 091101 (2011).
[3] J. Falson, Y. Kozuka, J. H. Smet, T. Arima, A. Tsukazaki, and M. Kawasaki, Appl. Phys. Lett. **107**, 082102 (2015).
[4] J. Falson, D. Maryenko, B. Friess, D. Zhang, Y. Kozuka, A. Tsukazaki, J. H. Smet, and M. Kawasaki, Nat. Phys. **11**, 347 (2015).
[5] Y. Kozuka, A. Tsukazaki, D. Maryenko, J. Falson, C. Bell, M. Kim, Y. Hikita, H. Y. Hwang, and M. Kawasaki, Phys. Rev. B **85**, 075302 (2012).
[6] G. Abstreiter, M. Cardona, and A. Pinczuk, *Light Scattering in Solids IV*, edited by M. Cardona and G. Guentherodt, Topics in Applied Physics Vol. 54 (Springer-Verlag, Berlin, 1984), pp. 5–150.
[7] A. Pinczuk, Adv. Solid State Phys. **32**, 45 (1992).
[8] L. V. Kulik and V. E. Kirpichev, Phys. Usp. **49**353 (2006).
[9] T. Makino, Y. Segawa, A. Tsukazaki, H. Saito, S. Takeyama, S. Akasaka, K. Nakahara, and M. Kawasaki, Phys. Rev. B **87**, 085312 (2013).
[10] V. V. Solovyev, A. B. Van'kov, I. V. Kukushkin, J. Falson, D. Zhang, D. Maryenko, Y. Kozuka, A. Tsukazaki, J. H. Smet, and M. Kawasaki, Appl. Phys. Lett. **106**, 082102 (2015).
[11] V. E. Kozlov, A. B. Van'kov, S. I. Gubarev, I. V. Kukushkin, V. V. Solovyev, J. Falson, D. Maryenko, Y. Kozuka, A. Tsukazaki, M. Kawasaki, and J. H. Smet, Phys. Rev. B **91**, 085304 (2015).
[12] M. R. Wagner, P. Zimmer, A. Hoffmann, and C. Thomsen, Physica Status Solidi (RRL) **1**, 169 (2007).
[13] I. V. Kukushkin and V. B. Timofeev, Adv. Phys. **45**, 147 (1996).
[14] J. E. Zucker, A. Pinczuk, D. S. Chemla, A. Gossard, and W. Wiegmann, Phys. Rev. Lett. **51**, 1293 (1983).
[15] A. Pinczuk, S. Schmitt-Rink, G. Danan, J. P. Valladares, L. N. Pfeiffer, and K. W. West, Phys. Rev. Lett. **63**, 1633 (1989).
[16] D. Gammon, B. V. Shanabrook, J. C. Ryan, and D. S. Katzer, Phys. Rev. B **41**, 12311(R) (1990).
[17] T. Ando, A. B. Fowler, and F. Stern, Rev. Mod. Phys. **54**, 437 (1982).
[18] S. Ernst, A. R. Goni, K. Syassen, and K. Eberl, Phys. Rev. Lett. **72**, 4029 (1994).